Global NEST Journal, Vol 22, No 1, pp 102-108

Investigation of ordered mesoporous carbon potential as CO_2 adsorbent

Çakman G.*, Ceylan S., Topcu Y., Geyikçi F.
Department of Chemical Engineering, Faculty of Engineering, Ondokuz Mayıs University, Atakum 55139, Samsun, Turkey
Received: 04/10/2018, Accepted: 17/02/2020, Available online: 20/02/2020
*to whom all correspondence should be addressed: e-mail: gulce.cakman@omu.edu.tr
https://doi.org/10.30955/gnj.002902

Abstract

In this study, an investigation was carried out in order to determine the potential of ordered mesoporous carbon including high ratio sucrose in its composition as a CO_2 adsorbent. Structural characterizations of silica and carbon material were determined by using a scanning electron microscope (SEM), N_2 adsorption/desorption and X-ray diffraction (XRD) analysis. CO_2 adsorption capacities of developed adsorbent at various temperatures (25 °C, 35 °C and 50 °C) were determined by using a thermogravimetric analyzer under CO_2 flow. The maximum adsorption capacity was obtained as approximately 2.27 mmol g CO_2 g^{-1} adsorbent which was remained almost the same in the desorption process. The first order reaction kinetic model was well fitted with the experimental data. Arrhenius equation was used to calculate activation energy which was obtained as -2.86 kJ mol^{-1} indicating barrier-less type adsorption. Results showed that ordered mesoporous carbon could be a potential source for an efficient and low-cost adsorbent for CO_2 capture.

Keywords: Ordered mesoporous carbon, CO_2 adsorption/desorption, kinetics.

1. Introduction

In recent years, greenhouse gases have become one of the most concern issues (Huang and Shen, 2013). The main factors of increasing greenhouse gas emission are economic and population growth. The environment has been affected negatively by the gas emissions such as increased global temperatures (0.12 °C per decade since 1951), ocean acidification (26% increase in acidity since 1750), and rising average sea levels (0.19 m since 1901) (Lashaki and Sayari, 2018). At the same time, if it doesn't take precaution for this, it is estimated that the global temperature will increase by 1-5 °C in 2050 (Liu *et al.*, 2017a; Villoria-Saez *et al.*, 2016). One of the main components of greenhouse gases is CO_2 and it is significantly produced from anthropogenic sources and fossil fuel combustion (Creamer *et al.*, 2016; Youn *et al.*, 2011). Also, it is reported that CO_2 contributes 60% of the total global warming caused by all greenhouse gases (Lakhi *et al.*, 2016). For all these reasons, researchers pay attention to CO_2 capture. Solvent absorption, pressure and temperature swing adsorption, membrane separation and cryogenic distillation have also been used to capture CO_2 (Pham *et al.*, 2016; Huang *et al.*, 2018; Yousef *et al.*, 2018). Nevertheless, some CO_2 capture processes have serious problems, such as energy penalties (Padurean *et al.*, 2013), economic and environmental drawbacks (Jing *et al.*, 2014; Ullah *et al.*, 2015) and amine waste during operation (Rochelle, 2009). To overcome such problems, the development of solid adsorbents to CO_2 capture has come to the prominence (Drage *et al.*, 2012). A large variety of adsorbents may be used for CO_2 captures, such as zeolites, microporous silicates, aluminum phosphates, carbons, other porous oxides, metal-organic frameworks (MOFs), amine-grafted or impregnated silica (Lashaki and Sayari, 2018; Ma *et al.*, 2018).

Solid adsorbents are very suitible for adsorption of CO_2 owing to high adsorption capacity, fast adsorption rate, and good stability (Liu *et al.*, 2017c). One of the solid adsorbents is porous carbon materials have been attracting lots of awareness as potential large-scale adsorbents because of the many advantages such as well-ordered structure, high surface area, large tunable and uniform mesoporous size, high mechanical strength and good hydrothermal stability at extensive temperature ranges (Zhao *et al.*, 2012; Deng *et al.*, 2012; Singh *et al.*, 2018; Liu *et al.*, 2017b). Carbons must have open pores to be accessible for the CO_2 molecules. Ryoo and co-workers (Ryoo *et al.*, 1999) prepared a new family of mesoporous carbons to represent as the CMK series. These carbon materials have a well-ordered pore structure with the larger surface area (Chandrasekar *et al.*, 2009). All of this properties made CMK series excellent applicant for hydrogen storage, gas separation, electrochemistry, catalysis, and adsorption (Juárez *et al.*, 2017; Yang *et al.*, 2018; Xu *et al.*, 2017). *Li and et al.* (2017) studied on CO_2 sorption over activated mesoporous carbon (AMC) and metal oxides (CeO_2, CuO, Mn_3O_4 and NiO) modified AMC with different pressure. The best result of CO_2 adsorption was 4.66 mmol/g at 273 K and 1 bar by using pure AMC as an adsorbent (Li *et al.*, 2017). *Chomiak and et al*. (2017) investigated that CO_2 adsorption on microporous granular

activated carbons (GACs) that has been prepared by KOH activation of walnut shell-based carbons. Carbons showed very high CO_2 adsorption, at 273 K up to 7.2 and 18.2 mmol/g under 1 and 30 bar, respectively (Chomiak *et al.*, 2017). *Ma et al.* (2018) studied CO_2 capture with nanoporous carbons materials which was prepared by using a metal-organic framework (MOF-5) as a template. The highest CO_2 adsorption capacity was obtained by nanoporous carbon that carbonized at 900 °C (3.70 mmol/g at 0 °C (1 atm)) (Ma *et al.*, 2018). In the study of *Pham et al.* (2016) nano-zeolite was evaluated for its potential use in CO_2 capture via temperature swing adsorption. As a result of the experiments, the best adsorption capacity of CO_2 by nano-zeolite was 4.81 mmol/g at a temperature of 20 °C and at a pressure of 1 atm (Pham *et al.*, 2016). *Lashaki et al.* (2018) examined the impact of the support pore structure on the CO_2 adsorption performance of triamine-tethered SBA-15 silica. Large-pore supports exhibited the highest surface density of amine groups (up to 35 μmol/m^2) and highest CO_2 uptakes (up to 1.88 mmol CO_2/g) (Lashaki and Sayari, 2018).

In most of the previous studies, adsorption isotherms of CO_2 adsorbents have been investigated and their adsorption capacities have been examined by various characterizing technics. However, there are few studies on CO_2 adsorption kinetics of such adsorbents. It is critical to examine adsorption kinetics, to better understand the events that occur during the adsorbent-goal material reaction, and also to estimate the time required to complete the adsorption process. Also, information on adsorbent characteristics and reaction kinetics is important for proper adsorbent selection, reactor sizing and process optimization. Thus, in this work we have carried out a comprehensive study both on CO_2 adsorption on to CMK-3 including characterization and kinetics.

In this study, it was carried out for the potential of the ordered mesoporous carbon to be used in carbon dioxide removal. SBA-15 was used as a template to synthesize ordered mesoporous carbon material, CMK-3, for CO_2 capture. Characterization of the adsorbent was carried out with different analytical instruments such as BET (Brunauer–Emmett–Teller), SEM (Scanning Electron Microscope), XRD (X-ray powder diffraction) and TGA (Thermogravimetric Analyzer). In addition, the mechanism of adsorption reaction was investigated and related kinetic parameters were calculated.

2. Materials and methods

2.1. Materials

Sucrose ($C_{12}H_{22}O_{11}$), pluronic 123 (P123), sulfuric acid (H_2SO_4) and hydrochloric acid (HCl) was supplied by Sigma-Aldrich. Tetraethylorthosilicate (TEOS) was purchased from Sigma-Aldrich with 97% purity. Hydrofluoric acid (HF) was supplied by Merck. The purity of hydrofluoric acid is 40%.

2.2. Synthesis of adsorbent

SBA-15 was synthesized according to Zhao *et al.* (1998). For the synthesis of CMK-3, sucrose ($C_{12}H_{22}O_{11}$), sulfuric acid and deionized water were used as a carbon source, acid solution, and solvent, respectively. CMK-3 was synthesized according to Jun *et al.* (2000). In briefly, 1.25 g sucrose, 5 g of deionized water and 0.14 g H_2SO_4 were stirred until a homogeneous solution was formed. 1 g of SBA-15 was added to this solution and continued to stir. The mixture was placed aged in a furnace at 100 °C for 6 hours and the furnace temperature was increased to 160 °C and maintained for 6 hours. 0.8 g sucrose, 0.08 g H_2SO_4 and 5 g of deionized water were added to this solution and were treated again for the same process (step 2). The resulting material was milled and carbonized in an inert atmosphere at 900 °C for 3 hours at 7 °C/min as a heating rate. After carbonization, the material was washed with HF and ionized water and dried overnight.

2.3. Characterization of adsorbent

The surface area, pore size, pore size distribution and pore volume values of synthesis samples were determined by using nitrogen adsorption/desorption isotherms. Nitrogen adsorption/desorption isotherms were studied by using Quantachrome Corporation, Autosorb.

Silica and carbon structures were investigated to use STOE IPDS II Model X-ray diffraction device. X-ray diffraction pattern of the synthesized sample, the step in the range of 0.02 and 0.025 (2θ/s) CuKα beam having a wavelength of 0.15406 nm were obtained. The characteristic peaks of silica and carbon were determined at 2θ between 1°-10°. Unit cell parameter (a_0), d100 spacing values (d_{100}) and pore wall thickness (δ) for SBA-15 and CMK-3 were calculated by using equation (1), equation (2) and equation (3), respectively. In equation (3), dp is pore diameter which is calculated by using the BJH method.

$$d_{100} = \frac{n\lambda}{2\sin\theta} \quad (1)$$

$$a_0 = \frac{2d100}{\sqrt{3}} \quad (2)$$

$$\delta = a - 0.95 \times dp \quad (3)$$

The morphologies of all the materials were observed using a scanning electron microscopy (SEM). The surfaces of silica structures were plated with a thin layer of gold-palladium before inspection under SEM. The SEM analysis was conducted with JEOL JSM-7001FTTLS LV SEM machine.

2.4. CO_2 adsorption experiments

CO_2 adsorption capacity was determined by DTA-TG Analysis unit (Shimadzu, Japan) (Creamer *et al.*, 2016). A sample weight of carbon approximately 20 mg was placed into an alumina sample pan. The placed sample was dried at 393 K for 1 h in a nitrogen atmosphere to potential volatile components out of the sample and then cooled down to room temperature. Nitrogen gas flow rate was 50 mL/min for both heating and cooling. When the system was at equilibrium, the CO_2 gas stream was switched on at a rate of 50 mL/min for 3 h. The adsorption capacity in percent was computed from the weight change of the sample in the TG adsorption process.

2.5. Kinetic studies

The CO_2 adsorption kinetics onto carbon adsorbent can be described using various kinetic model such as pseudo-first order (Eq. 4) and pseudo-second order (Eq. 5) model (Simonin, 2016).

$$\frac{dq_t}{dt} = k_1 \times (q_e - q_t) \quad (4)$$

$$\frac{dq_t}{dt} = k_2 \times (q_e - q_t)^2 \quad (5)$$

Where q_t (mg g^{-1}) and q_e (mg g^{-1}) are the concentrations of CO_2 adsorption at time t and at equilibrium, respectively, k_1 and k_2 (g mg^{-1} s^{-1}) is the first and second-order adsorption rate constants.

The activation energy must be minimum value in order to facilitate the adsorption process. The activation energy can be calculated using the Arrhenius equation shown in equation (6) (Shahrom *et al.*, 2018).

$$\ln k = \ln A - \frac{E_a}{RT} \quad (6)$$

According to equation (6), k_1 is the rate constant, A is the temperature impact factor, E_a is the activation energy for adsorption (J/mol), R is the gas constant (8.314 J/mol K) and T is the adsorption temperature in K.

3. Result and discussion

3.1. Characterizations of carbon materials

The ordered pore structure, surface area and morphological structure of the synthesized adsorbent were determined by XRD, nitrogen adsorption/desorption isotherm and SEM, respectively.

3.1.1. N_2 adsorption/desorption

The textural parameters of SBA-15 and CMK-3 samples are investigated using N_2 adsorption/desorption technique. The textural parameters of these samples including the specific surface area, specific pore volume, and average pore size are summarized in Table 1. The specific surface area and total pore volume of the CMK-3 are 1360 m^2/g and 1.167 cm^3/g, respectively. These results are consistent with the literature (Huang and Shen, 2013; Ghani *et al.*, 2015).

Table 1. Textural property of SBA-15 and CMK-3

Adsorbents	BET surface area (m^2/g)	Total pore volume (cm^3/g)	BJH method average pore size (nm)	SF method average pore size (nm)
SBA-15	753	1.285	3.9	0.47
CMK-3	1360	1.167	2.03	0.46

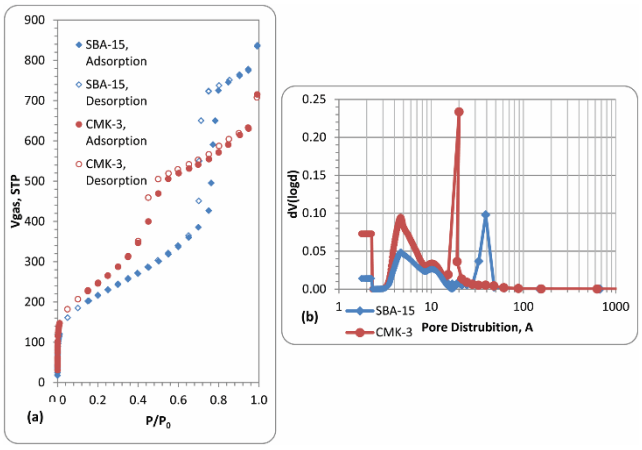

Figure 1. (a) N_2 adsorption/desorption isotherms. (b) Pore distributions of SBA-15 and CMK-3

Figure 1 shows the N_2 adsorption/desorption isotherms and pore distributions of samples. The synthesized SBA-15 and CMK-3 have been shown to exhibit Type IV isotherm behavior in the BDDT (Brunauer-Deming-Deming-Teller) classification as in the literature (Araujo *et al.*, 2016; Tang *et al.*, 2017). According to Figure 1a, SBA-15 and CMK-3 samples prove to have a mesopore structure. It also shows that in addition to mesoporosity, the structures also have microporosity. From the adsorption/desorption isotherms, the hysteresis loop for the SBA-15 and CMK-3 samples are observed at partial pressure values in the range of 0.65-0.80 and 0.45-0.6 for P/P_0, respectively. This type of hysteresis (H1 hysteresis) shows that the structure has a cylindrical structure (Alothman, 2012). The sharp increase and decrease in the hysteresis region is indicative of the narrow pore size distribution in accordance with the pore size distribution shown in Figure 1b. The pore size distributions shown in Figure 1b are performed by the BJH method for mesopore and SF method for micropore. The average pore size of CMK-3 is 2.03 nm.

3.1.2. Small angle X-ray diffraction

Figure 2 shows the small angle powder XRD patterns of SBA-15 and CMK-3 samples. The SAXS patterns of SBA-15 show the dominant signal peak corresponding to the (100) plane and two small diffraction peaks at higher angles (110) and (200) plane, characteristic of a well-defined hexagonal 2D structures of P6mm symmetry (Sareen *et al.*, 2016; Ochoa-Hernández *et al.*, 2013). CMK-3 was obtained from pore filling of SBA-15 and uniform hexagonal carbon rods were formed. The CMK-3 sample provides a diffractogram with a dominant peak corresponding to the (100) plane, characteristic of these kinds of ordered mesoporous carbons (Joo *et al.*, 2002). This shows that CMK-3 succesfully replicate SBA-15 templates. The patterns for both SBA-15 and CMK-3 indicate that they are ordered mesoporous materials with well-defined pore geometry.

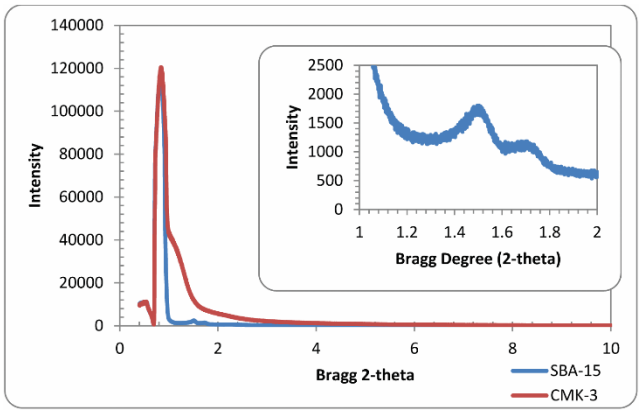

Figure 2. XRD Patterns of SBA-15 and CMK-3

Unit cell parameter (a_0), d100 spacing values (d100) and pore wall thickness (δ) of all materials are given in Table 2. The wall thickness of the SBA-15 and CMK-3 sample was calculated at 8.91 nm and 10.38 nm, respectively. It was found to be consistent with the wall thickness (3-9 nm) specified in the literature (Zhao *et al.*, 1998; Meynen *et al.*, 2009).

Table 2. Unit cell parameter (a_0), d100 spacing values (d100) and pore wall thickness (δ)

Adsorbents	d (nm)	a (nm)	δ (nm)
SBA-15	10.63	12.61	8.91
CMK-3	10.64	12.28	10.38

3.1.3. SEM images

The morphology of SBA-15 and CMK-3 are illustrated in Figure 3. SBA-15 structures are formed homogeneously. SEM images have proven that CMK-3 is synthesized without change of the surface morphology of SBA-15. SBA-15 and CMK-3 structures have rod-type morphology. The obtained SEM images of SBA-15 and CMK-3 are good agreement with literature (Radhakrishnan *et al.*, 2017; Zhu *et al.*, 2019). EDX analysis of these materials shows that the template has only silica for SBA-15 and the CMK-3 sample has only carbon, confirming the success of the synthesis.

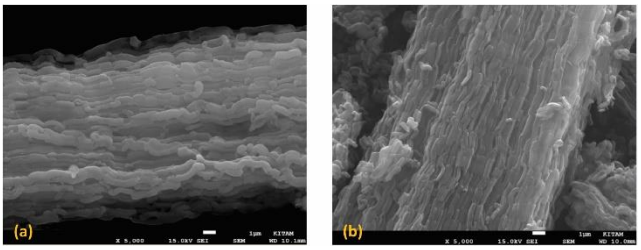

Figure 3 SEM images of (a) SBA-15 and (b) CMK-3

3.2. Kinetic studies of CO_2 adsorption on the carbon material

The TGA data on the CO_2 adsorption capacity of CMK-3 at 25 °C, 35 °C and 50 °C are shown in Figure 4. It has been found that different CO_2 adsorption capacities at various temperatures. Because of CO_2 adsorption is an exothermic reaction, lower temperature is most suitable for CO_2 adsorption. The highest adsorption capacity is obtained at 25 °C as approximately 2.27 mmol CO_2/g adsorbent. This indicates that the higher driving force at 25 °C. As seen from Table 3, the adsorption capacity of the produced adsorbent is within the range of previously reported ones. Thus it can be said that this type of adsorbent have a potential for CO_2 capture processes.

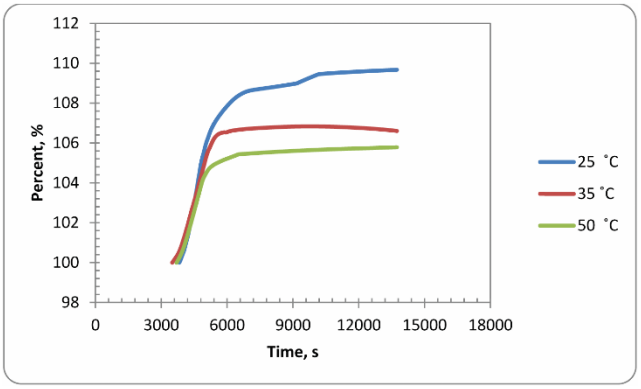

Figure 4. CO_2 adsorption capacity of CMK-3 with various temperatures

Table 3. Comparison of adsorption capacities with literature

Material	Condition	Capacity (mmol/g)	Reference
Activated carbon	273 K and 1 bar	4.66	Li *et al.* (2017)
PEHA-loaded SBA-16	343 K and 1 atm	2.1	Wu *et al.* (2018)
KOH activated walnut shell-based carbons	273 K and 1 bar	7.2	Chomiak *et al.* (2017)
Metal-organic framework	273 K and 1 atm	3.70	Ma *et al.* (2018)
Nano zeolite	293 K and 1 atm	4.81	Pham *et al.* (2016)
Nano structured carbon	303 K and 1 atm	1.5	Tiwari *et al.* (2018)
Amine activated kenaf		2.086	Kamarudin *et al.* (2018)
Palm activated char	303 K and 1 bar	1.66	Nasri *et al.* (2014)
Al salt activated cottonwood	298 K and 1 bar	1.61	Creamer *et al.* (2016)
CMK-3	298 K and 1 atm	2.27	*This study*

CO_2 adsorption kinetics is determined by using different adsorption kinetic models such as pseudo-first-order and pseudo-second-order. The pseudo-second-order model poorly fits into the kinetic data in which low R^2 *values were obtained.* For this reason, the pseudo-first-order model can describe the adsorption process of CO_2 on carbon adsorbent. Kinetic parameters at various temperatures are given in Figure 5a. Pseudo-first order fits the CO_2 adsorption at all temperatures with high regression coefficient values (>0.90). With the increase in

temperature, decrease in rate constant which indicates an exothermic process. The rate constant at 25 °C, 35 °C and 50 °C are 0.0030103 s^{-1}, 0.0028958 s^{-1} and 0.0027798 s^{-1}, respectively.

The *lnk* has been plotted versus the inverse of temperature (1/T) to determining the activation energy at Figure 5b. The value of activation energy is found -2.86 kJ/mol. The activation energy is negative because the reaction rate decreases as the temperature increases. CO_2 adsorption with negative activation energy is categorized as barrier-less adsorption. This adsorption process depends on the capture of CO_2 molecules in a potential well.

In this case, the probability of collision of CO_2 molecules decreases as the temperature increases (Liu *et al.*, 2014). The activation energy value of different adsorbents is given in Table 4. The activation energy of CMK-3 for CO_2 adsorption showed similarity with literature.

Table 4. Activation energy of CO_2 adsorption for various adsorbent

Adsorbent	Activation energy (kJ/mol)	References
Activated carbon	-2.28	Wei *et al.* (2017)
Thermally treated graphene nanosheets	-7.21	Kudahi *et al.* (2017)
Amine functionalized KIT-6*	-6.56	Liu and Yu (2018)
CMK-3	-2.86	In this study

*****CO_2 *concentration (vol %60)*

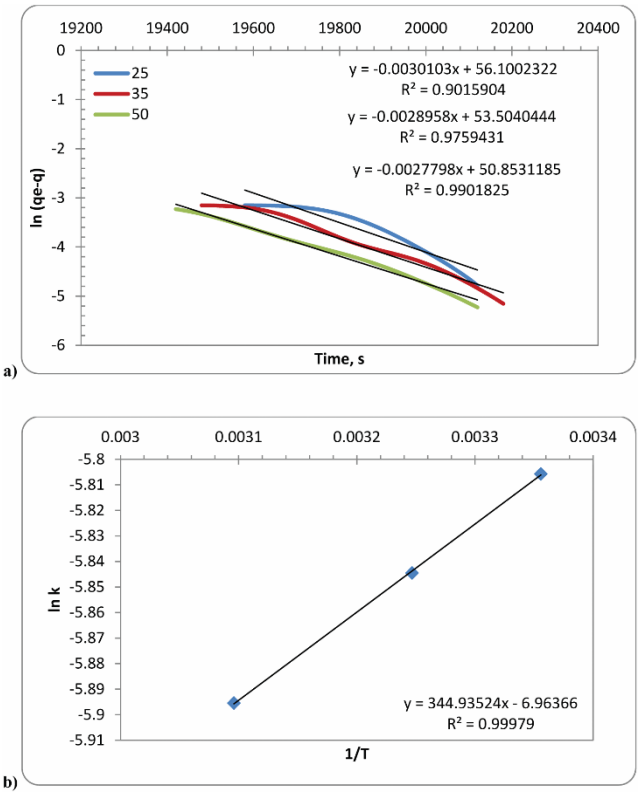

Figure 5. a) Kinetic plot of pseudo first order model with various temperatures. b) Arrhenius plot for activation energy calculation

3.3. CO_2 desorption on the carbon material

Reusability is one of the most important parameters for adsorbents. For this reason, the reusability of CMK-3 for CO_2 adsorption is also studied at 25 °C. Desorption process carried out an inert atmosphere (N_2 flow) after CO_2 adsorption. This adsorption/desorption cycle was repeated two times and distinguished variety are not observed in the CO_2 desorption or adsorption. As seen in Figure 6, similar curves for both fresh and regenerated adsorbents and this indicates that the CO_2 adsorption capacity is the almost the same. Therefore, CMK-3 can be reported as fast, easily, and completely regenerated over multiple cycles without noticeable loss of adsorption capacity.

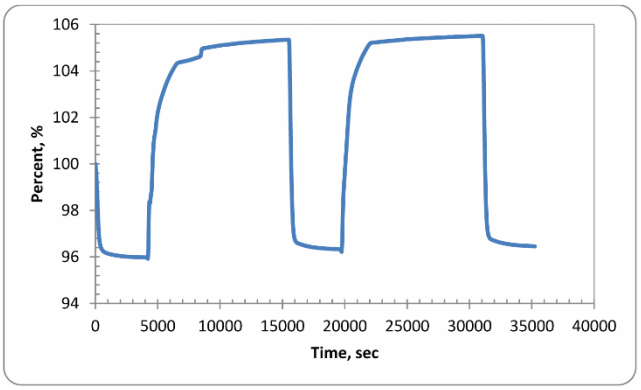

Figure 6. CO_2 adsorption and desorption capacity of CMK-3

4. Conclusion

In this study, CMK-3 has been synthesized and characterized in order to evaluate the potential of ordered mesoporous carbon as a CO_2 adsorbent. According to the characterization, CMK-3 was succesfully synthesis from pore filling of SBA-15. The adsorption capacity reduced with increase in temperature. The highest adsorption capacity is obtained at 25 °C as approximately 2.27 mmol CO_2/g adsorbent. Kinetic parameters were evaluated with pseudo-first order kinetics where a negative value of activation energy obtained indicating barrier-less type CO_2 capture process. The desorption performance of the adsorbent was almost same the adsorption capacity. Results showed that ordered mesoporous carbon, CMK-3, has a potential in efficient CO_2 adsorbent.

Acknowledgements

This research did not receive any specific grant from funding agencies in the public, commercial, or not-for-profit sectors.

References

Alothman Z.A. (2012), A review: fundamental aspects of silicate mesoporous materials, *Materials*, **5**, 2874–2902.

Araujo M., Silva L., Sczancoski J., Orlandi M., Longo E., Santos A., Sa J., Santos R., Luz Jr G. and Cavalcante L. (2016), Anatase TiO2 nanocrystals anchored at inside of SBA-15 mesopores

and their optical behavior, *Applied Surface Science*, **389**, 1137–1147.

Chandrasekar G., Son W.-J. and Ahn W.-S. (2009), Synthesis of mesoporous materials SBA-15 and CMK-3 from fly ash and their application for CO2 adsorption, *Journal of porous materials*, **16**, 545–551.

Chomiak K., Gryglewicz S., Kierzek K. and Machnikowski J. (2017), Optimizing the properties of granular walnut-shell based KOH activated carbons for carbon dioxide adsorption, *Journal of CO2 Utilization*, **21**, 436–443.

Creamer A.E., Gao B. and Wang S. (2016), Carbon dioxide capture using various metal oxyhydroxide–biochar composites, *Chemical Engineering Journal*, **283**, 826–832.

Deng Q.-F., Liu L., Lin X.-Z., Du G., Liu Y. and Yuan Z.-Y. (2012), Synthesis and CO2 capture properties of mesoporous carbon nitride materials, *Chemical Engineering Journal*, **203**, 63–70.

Drage T.C., Snape C.E., Stevens L.A., Wood J., Wang J., Cooper A.I., Dawson R., Guo X., Satterley C. and Irons R. (2012), Materials challenges for the development of solid sorbents for post-combustion carbon capture, *Journal of Materials Chemistry*, **22**, 2815–2823.

Ghani K., Kiomarsipour N. and Jaberi H. (2015), Evaluation of optical properties of CMK-1 and CMK-3 mesoporous carbons and introduction them as very interesting black pigments, *Dyes and Pigments*, **122**, 126–133.

Huang A., Chen L.-H., Chen C.-H., Tsai H.-Y. and Tung K.-L. (2018), Carbon dioxide capture using an omniphobic membrane for a gas-liquid contacting process, *Journal of Membrane Science*, **556**, 227–237.

Huang C.-C. and Shen S.-C. (2013), Adsorption of CO2 on chitosan modified CMK-3 at ambient temperature, *Journal of the Taiwan Institute of Chemical Engineers*, **44**, 89–94.

Jing Y., Wei L., Wang Y. and Yu Y. (2014), Synthesis, characterization and CO2 capture of mesoporous SBA-15 adsorbents functionalized with melamine-based and acrylate-based amine dendrimers, *Microporous and Mesoporous Materials*, **183**, 124–133.

Joo S.H., Ryoo R., Kruk M. and Jaroniec M. (2002), Evidence for general nature of pore interconnectivity in 2-dimensional hexagonal mesoporous silicas prepared using block copolymer templates, *The Journal of Physical Chemistry B*, **106**, 4640–4646.

Juárez J.M., Ledesma B.C., Costa M.G., Beltramone A.R. and Anunziata O.A. (2017), Novel preparation of CMK-3 nanostructured material modified with titania applied in hydrogen uptake and storage, *Microporous and Mesoporous Materials*, **254**, 146–152.

Jun S., Joo S.H., Ryoo R., Kruk M., Jaroniec M., Liu Z., Ohsuna T. and Terasaki O. (2000), Synthesis of new, nanoporous carbon with hexagonally ordered mesostructure, *Journal of the American Chemical Society*, **122**, 10712–10713.

Kamarudin K., Zaini N. and Khairuddin N. (2018), CO2 removal using amine-functionalized kenaf in pressure swing adsorption system, *Journal of Environmental Chemical Engineering*, **6**, 549–559.

Kudahi S.N., Noorpoor A.R. and Mahmoodi N.M. (2017), Determination and analysis of CO2 capture kinetics and mechanisms on the novel graphene-based adsorbents, *Journal of CO2 Utilization*, **21**, 17–29.

Lakhi K.S., Cha W.S., Choy J.-H., Al-Ejji M., Abdullah A.M., Al-Enizi A.M. and Vinu A. (2016), Synthesis of mesoporous carbons with controlled morphology and pore diameters from SBA-15 prepared through the microwave-assisted process and their CO2 adsorption capacity, *Microporous and Mesoporous Materials*, **233**, 44–52.

Lashaki M.J. and Sayari A. (2018), CO2 capture using triamine-grafted SBA-15: The impact of the support pore structure, *Chemical Engineering Journal*, **334**, 1260–1269.

Li M., Huang K., Schott J.A., Wu Z. and Dai S. (2017), Effect of metal oxides modification on CO2 adsorption performance over mesoporous carbon, *Microporous and Mesoporous Materials*, **249**, 34–41.

Liu Q., Shi J., Zheng S., Tao M., He Y. and Shi Y. (2014), Kinetics studies of CO2 adsorption/desorption on amine-functionalized multiwalled carbon nanotubes, *Industrial & Engineering Chemistry Research*, **53**, 11677–11683.

Liu X., Zhai X., Liu D. and Sun Y. (2017a), Different CO2 absorbents-modified SBA-15 sorbent for highly selective CO2 capture, *Chemical Physics Letters*, **676**, 53–57.

Liu Y., Chen Y., Tian L. and Hu R. (2017b), Hierarchical porous nitrogen-doped carbon materials derived from one-step carbonization of polyimide for efficient CO2 adsorption and separation, *Journal of Porous Materials*, **24**, 583–589.

Liu Y., Lin X., Wu X., Liu M., Shi R. and Yu X. (2017c), Pentaethylenehexamine loaded SBA-16 for CO2 capture from simulated flue gas, *Powder Technology*, **318**, 186–192.

Liu Y. and Yu X. (2018), Carbon dioxide adsorption properties and adsorption/desorption kinetics of amine-functionalized KIT-6, *Applied Energy*, **211**, 1080–1088.

Ma X., Li L., Chen R., Wang C., Li H. and Wang S. (2018), Heteroatom-doped nanoporous carbon derived from MOF-5 for CO2 capture, *Applied Surface Science*, **435**, 494–502.

Meynen V., Cool P. and Vansant E.F. (2009), Verified syntheses of mesoporous materials, *Microporous and Mesoporous Materials*, **125**, 170–223.

Nasri N.S., Hamza U.D., Ismail S.N., Ahmed M.M. and Mohsin R. (2014), Assessment of porous carbons derived from sustainable palm solid waste for carbon dioxide capture, *Journal of Cleaner Production*, **71**, 148–157.

Ochoa-Hernández C., Yang Y., Pizarro P., A. Víctor, Coronado J.M. and Serrano D.P. (2013), Hydrocarbons production through hydrotreating of methyl esters over Ni and Co supported on SBA-15 and Al-SBA-15, *Catalysis Today*, **210**, 81–88.

Padurean A., Cormos C.-C. and Şerban Agachi P. (2013), Techno-economical evaluation of post-and pre-combustion carbon dioxide capture methods applied for an igcc power generation plant, *Environmental Engineering & Management Journal (EEMJ)*, **12**.

Pham T.-H., Lee B.-K., Kim J. and Lee C.-h. (2016), Enhancement of CO2 capture by using synthesized nano-zeolite, *Journal of the Taiwan Institute of Chemical Engineers*, **64**, 220–226.

Radhakrishnan R., Thiripuranthagan S., Devarajan A., Kumaravel S., Erusappan E. and Kannan K. (2017), Oxidative esterification of furfural by Au nanoparticles supported CMK-3 mesoporous catalysts, *Applied Catalysis A: General*, **545**, 33–43.

Rochelle G.T. (2009), Amine scrubbing for CO2 capture, *Science*, **325**, 1652–1654.

Ryoo R., Joo S.H. and Jun S. (1999), Synthesis of highly ordered carbon molecular sieves via template-mediated structural transformation, *The Journal of Physical Chemistry B*, **103**, 7743–7746.

Sareen S., Mutreja V., Singh S. and Pal B. (2016), Fine CuO anisotropic nanoparticles supported on mesoporous SBA-15 for selective hydrogenation of nitroaromatics, *Journal of Colloid and Interface Science*, **461**, 203–210.

Shahrom M.S.R., Wilfred C.D. and Chong F.K. (2018), Thermodynamic and kinetic studies on CO2 capture with Poly [VBTMA][Arg], *Journal of Physics and Chemistry of Solids*, **116**, 22–29.

Simonin J.-P. (2016), On the comparison of pseudo-first order and pseudo-second order rate laws in the modeling of adsorption kinetics, *Chemical Engineering Journal*, **300**, 254–263.

Singh G., Lakhi K.S., Ramadass K., Kim S., Stockdale D. and Vinu A. (2018), A combined strategy of acid-assisted polymerization and solid state activation to synthesize functionalized nanoporous activated biocarbons from biomass for CO2 capture, *Microporous and Mesoporous Materials*, **271**, 23–32.

Tang W., Deng Y. and Chen Y. (2017), Promoting effect of acid treatment on Pd-Ni/SBA-15 catalyst for complete oxidation of gaseous benzene, *Catalysis Communications*, **89**, 86–90.

Tiwari D., Kaur S., Bhunia H. and Bajpai P.K. (2018), CO2 adsorption on oxygen enriched nanostructured carbons derived from silica templated resorcinol-formaldehyde, *Journal of Industrial and Engineering Chemistry*.

Ullah R., Atilhan M., Aparicio S., Canlier A. and Yavuz C.T. (2015), Insights of CO2 adsorption performance of amine impregnated mesoporous silica (SBA-15) at wide range pressure and temperature conditions, *International Journal of Greenhouse Gas Control*, **43**, 22–32.

Villoria-Saez P., Tam V.W., del Río Merino M., Arrebola C.V. and Wang X. (2016), Effectiveness of greenhouse-gas Emission Trading Schemes implementation: a review on legislations, *Journal of Cleaner Production*, **127**, 49–58.

Wei M., Yu Q., Xie H., Zuo Z., Hou L. and Yang F. (2017), Kinetics studies of CO2 adsorption and desorption on waste ion-exchange resin-based activated carbon, *International Journal of Hydrogen Energy*, **42**, 27122–27129.

Wu X., Liu M., Shi R., Yu X. and Liu Y. (2018), CO2 adsorption/regeneration kinetics and regeneration properties of amine functionalized SBA-16, *Journal of Porous Materials*, 1–9.

Xu Y., Li Y., Wang C., Wang C., Ma L., Wang T., Zhang X. and Zhang Q. (2017), In-situ hydrogenation of model compounds and raw bio-oil over Ni/CMK-3 catalyst, *Fuel Processing Technology*, **161**, 226–231.

Yang Y., Wang J., Qian X., Shan Y. and Zhang H. (2018), Aminopropyl-functionalized mesoporous carbon (APTMS-CMK-3) as effective phosphate adsorbent, *Applied Surface Science*, **427**, 206–214.

Youn H.-K., Kim J., Chandrasekar G., Jin H. and Ahn W.-S. (2011), High pressure carbon dioxide adsorption on nanoporous carbons prepared by Zeolite Y templating, *Materials Letters*, **65**, 1772–1774.

Yousef A.M., El-Maghlany W.M., Eldrainy Y.A. and Attia A. (2018), New Approach for Biogas Purification using Cryogenic Separation and Distillation Process for CO2 Capture, *Energy*.

Zhao D., Feng J., Huo Q., Melosh N., Fredrickson G.H., Chmelka B.F. and Stucky G.D. (1998), Triblock copolymer syntheses of mesoporous silica with periodic 50 to 300 angstrom pores, *Science*, **279**, 548–552.

Zhao Y., Zhao L., Yao K.X., Yang Y., Zhang Q. and Han Y. (2012), Novel porous carbon materials with ultrahigh nitrogen contents for selective CO2 capture, *Journal of Materials Chemistry*, **22**, 19726–19731.

Zhu G., Wang L., Zhang Y., Yu W. and Xie H. (2019), Au–Ag alloy nanoparticles supported on ordered mesoporous carbon (CMK-3) with remarkable solar thermal conversion efficiency, *Applied Physics A*, **125**, 151.